# Time-dependent density functional theory quantum transport simulation in non-orthogonal basis

Yan Ho Kwok, Hang Xie, Chi Yung Yam, Xiao Zheng, and Guan Hua Chen

---

**Articles you may be interested in**

Time-dependent density functional theory for quantum transport
J. Chem. Phys. **133**, 114101 (2010); 10.1063/1.3475566

Time-dependent transport through molecular junctions
J. Chem. Phys. **132**, 234105 (2010); 10.1063/1.3435351

Real-time, local basis-set implementation of time-dependent density functional theory for excited state dynamics simulations
J. Chem. Phys. **129**, 054110 (2008); 10.1063/1.2960628

Linear optical response of current-carrying molecular junction: A nonequilibrium Green's function–time-dependent density functional theory approach
J. Chem. Phys. **128**, 124705 (2008); 10.1063/1.2876011

A model study of quantum dot polarizability calculations using time-dependent density functional methods
J. Chem. Phys. **106**, 4543 (1997); 10.1063/1.473497

---

# Time-dependent density functional theory quantum transport simulation in non-orthogonal basis

Yan Ho Kwok,[1] Hang Xie,[1] Chi Yung Yam,[1] Xiao Zheng,[2] and Guan Hua Chen[1,a]

[1]*Department of Chemistry, The University of Hong Kong, Pokfulam Road, Hong Kong*
[2]*Hefei National Laboratory for Physical Sciences at the Microscale, University of Science and Technology of China, Hefei, Anhui 230026, China*

Basing on the earlier works on the hierarchical equations of motion for quantum transport, we present in this paper a first principles scheme for time-dependent quantum transport by combining time-dependent density functional theory (TDDFT) and Keldysh's non-equilibrium Green's function formalism. This scheme is beyond the wide band limit approximation and is directly applicable to the case of non-orthogonal basis without the need of basis transformation. The overlap between the basis in the lead and the device region is treated properly by including it in the self-energy and it can be shown that this approach is equivalent to a lead-device orthogonalization. This scheme has been implemented at both TDDFT and density functional tight-binding level. Simulation results are presented to demonstrate our method and comparison with wide band limit approximation is made. Finally, the sparsity of the matrices and computational complexity of this method are analyzed. © *2013 AIP Publishing LLC*. [http://dx.doi.org/10.1063/1.4840655]

## I. INTRODUCTION

Given the rapid development of nanoscale electronics[1–7] and the possibility of measuring transient current experimentally,[8] time-dependent quantum transport has become an interesting research topic since it allows us to investigate transient dynamics of molecules coupled with environment under time-dependent perturbation. In particular, we are interested in first principles simulation with atomistic details in which no empirical parameters are required.

To simulate time-dependent quantum transport, one popular approach is to combine Keldysh's non-equilibrium Green's function (NEGF) formalism with time-dependent density functional theory (TDDFT)[9–20] so that one can work with a non-interacting reference system and use single-particle Green's function to formulate the problem. In particular, we have developed a reduced single-electron density matrix (RSDM) based TDDFT-NEGF-hierarchical equations of motion (HEOM) formalism,[10] which is in principle exact and the hierarchy is closed at the 2nd tier within the TDDFT framework. The hierarchical equation of motion method involves solving for the time evolution of the reduced density operator with the help of auxiliary density operators, which are arranged in a hierarchical structure.[21] The 1st tier auxiliary matrices are time-dependent unknowns that appear in the equation of motion of RSDM. And when we attempt to derive the equations of motion for these 1st tier auxiliary matrices, another set of unknown matrices appear and they are called the 2nd tier auxiliary matrices. This process continues and we thus have a hierarchical structure of auxiliary matrices. For non-interacting system, such as the Kohn Sham reference system in the TDDFT framework, the hierarchy is terminated at 2nd tier exactly. If the wide-band limit (WBL) approximation

is made, the RSDM based HEOM can be closed at 1st tier.[10, 22] Beyond the WBL, the RSDM based HEOM have been applied to simulate time-dependent quantum transport in tight-binding model system.[23, 24]

However, in the derivation of RSDM based HEOM, a localized orthonormal basis set is assumed. In practical first principles calculation, atomic orbital basis, which are the eigenfunctions of the single-electron Hamiltonian of individual atoms, are commonly used due to their localized nature and clear chemical meaning. Atomic orbital basis is a non-orthogonal basis since atomic orbitals belonging to different atoms are in general non-orthogonal to each other. In electron transport simulation, the locality of the basis set in real space is especially essential since it permits us to partition the matrices into blocks corresponding to lead or device regions. Although there exist relatively localized orthogonal basis sets such as the wavelet basis[25–27] and the localized molecular orbitals[28, 29] (Wannier functions[30, 31]) commonly used in linear scaling methods, they are certainly not as localized as atomic orbitals and they often extend over several atoms.

Applying formalism derived in orthogonal basis to the case of non-orthogonal basis is not straightforward due to the lead-device basis overlap. The lead-device basis overlap leads to a significantly different expression for the self-energy and complicates the derivation. For steady state (energy-domain) calculation, the Laudauer formula remains the same in terms of the self-energies and device Green's function but we have to take into account the overlap matrix when calculating the self-energies and Green's functions.[32–36] For time-domain simulation, the extension to non-orthogonal basis is less straightforward. Also, due to the overlap among the basis sets in different sub-regions, there is ambiguity in defining the number of electrons in each sub-regions and so does the current.[37, 38] A common practice to deal with the problem of non-orthogonal basis is to do some kinds of basis

a)Electronic mail: ghc@everest.hku.hk

transformation before partitioning the system. One may transform the whole system to orthogonal basis[18] but this has to be done with care so that the periodicity of the lead is preserved and the basis set remains as localized as possible. Another way to avoid the lead-device overlap is to transform the basis associated with the device region to another one that is orthogonal to the lead basis.[39]

In this paper, we attempt to solve the problem by examining the property of self-energy in non-orthogonal basis and extending the TDDFT-NEGF-HEOM formalism to non-orthogonal basis so that the atomic orbital basis can be directly used in time-dependent simulation.

This paper is organized as follows: first, we derive the RSDM based HEOM in non-orthogonal basis. Second, we show that our results are equivalent to a lead-device orthogonalization (i.e., making the basis in device region orthogonal to the basis in the leads). Third, details of implementation are outlined and results are presented to confirm our method. Finally, the computational complexity as well as memory requirement will be discussed.

## II. THEORY

Under the TDDFT formalism, we follow the dynamics of a non-interacting reference system with the Hamiltonian

$$H(t) = \sum_{i=1}^{N} h(\vec{r}_i, t) = \sum_{i=1}^{N} \left( -\frac{1}{2}\nabla_i^2 + \upsilon_{KS}(\vec{r}_i, t) \right), \quad (1)$$

where $\upsilon_{KS}(\vec{r}, t) = \upsilon_{ext}(\vec{r}, t) + \upsilon_H(\vec{r}, t) + \upsilon_{xc}(\vec{r}, t)$ is the effective Kohn-Sham potential including external potential, mean field electron-electron repulsion as well as exchange-correlation (XC) potential. In principle, given the exact XC functional, this reference system will evolve in a way that produces the exact electron density $\rho(\vec{r}, t)$ according to Runge-Gross theorem.[40] We expand our reference system by a non-orthogonal atomic basis set $\{\chi_\mu\}$ such that the Kohn-Sham Fock matrix in covariant representation is given by $h_{\mu\nu} = \langle \chi_\mu | \hat{h} | \chi_\nu \rangle$. The reduced single-electron density matrix $\sigma_{\mu\nu}$ of the reference system is then defined as the contravariant representation of the reduced single-electron density operator

$$\hat{\sigma} = \sum_{\mu\nu} \sigma_{\mu\nu} |\chi_\nu\rangle\langle\chi_\mu|. \quad (2)$$

The RSDM for isolated system obeys the equation of motion

$$i S \dot{\sigma}(t) S = h(t)\sigma(t)S - S\sigma(t)h(t), \quad (3)$$

where $S_{\mu\nu} = \langle \chi_\mu | \chi_\nu \rangle$ is the overlap matrix, the covariant representation of identity matrix in a non-orthogonal basis. In orthogonal basis, this equation of motion reduces to $i\dot{\sigma}(t) = [h(t), \sigma(t)]$.

In quantum transport simulation, we are interested in the particular lead-device-lead set up as shown in Fig. 1. We would like to follow the evolution of the device region while the leads are treated as environment. Since our system is expanded by a localized basis set, we can partition all the matrices into blocks corresponding to the respective regions in real
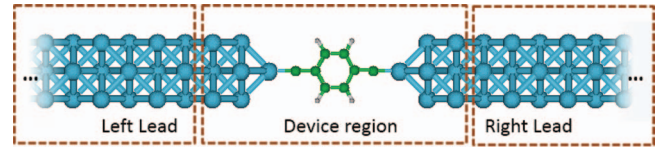


FIG. 1. Schematic diagram showing the partitioning of entire system into three regions: left-lead, device, and right lead.

space. For instance,

$$h = \begin{bmatrix} h_L & h_{LD} & 0 \\ h_{DL} & h_D & h_{DR} \\ 0 & h_{LD} & h_R \end{bmatrix},$$

where $L$, $R$, and $D$ denote the left lead, right lead, and device, respectively. We assumed that different leads do not couple directly with each other, thus $h_{LR} = S_{LR} = 0$. It is noted that the matrices $h_L$, $h_R$, etc., are of infinite dimension representing the semi-infinite leads which contain infinite degree of freedom. Therefore, deriving the equation of motion for $\sigma_D(t)$ is an open system problem.

### A. NEGF in non-orthogonal basis

The equation of motion for $\sigma_D(t)$ can be derived based on the Keldysh's NEGF formalism, in which $\sigma_D(t)$ is equivalent to the lesser Green's function $G_{ij}^<(t, t') = i \langle a^{j\dagger}(t')a^i(t) \rangle$ at $t = t'$, where $a^{i\dagger}(t)$, $a^i(t)$ are the Heisenberg creation and annihilation operators in duel basis (see Appendix A for details),

$$\sigma_D(t) = -i G_D^<(t, t). \quad (4)$$

With Dyson's equation and analytical continuation rules of Langreth, the equation of motion for $G_D^<(t, t')$ is shown to be

$$i S_D \frac{\partial}{\partial t} G_D^<(t, t') = h_D(t) G_D^<(t, t')$$
$$+ \sum_\alpha \int_{-\infty}^{\infty} d\tau \left[ \Sigma_\alpha^r(t, \tau) G_D^<(\tau, t') \right.$$
$$\left. + \Sigma_\alpha^<(t, \tau) G_D^a(\tau, t') \right]. \quad (5)$$

The superscripts $r$, $a$, $<$, $>$ indicate the retarded, advanced, lesser, and greater component of the non-equilibrium Green's function or self-energies. And the self-energies describing the coupling and overlapping with lead $\alpha$ are given by

$$\Sigma_\alpha^x(t_1, t_2)$$

$$= \left( h_{D\alpha}(t_1) - i S_{D\alpha} \frac{\overrightarrow{\partial}}{\partial t_1} \right) g_\alpha^x(t_1, t_2) \left( h_{\alpha D}(t_2) - i S_{\alpha D} \frac{\overrightarrow{\partial}}{\partial t_2} \right)$$

$$= \left( h_{D\alpha}(t_1) - i S_{D\alpha} \frac{\overrightarrow{\partial}}{\partial t_1} \right) g_\alpha^x(t_1, t_2) \left( h_{\alpha D}(t_2) + i S_{\alpha D} \frac{\overleftarrow{\partial}}{\partial t_2} \right), \quad (6)$$

where $x = r, a, <, >$ and $\frac{\overleftarrow{\partial}}{\partial t}$, $\frac{\overrightarrow{\partial}}{\partial t}$ denote the left and right derivatives, respectively. The small letter $g(t, t')$ is the bare

Green's function for a corresponding uncoupled system in which the leads and device region are isolated from each others, i.e., $S_{D\alpha}, h_{D\alpha} = 0$.

The 1st equality in Eq. (6) is obtained by partitioning the Dyson's equation and its derivation is similar to the derivation in energy-domain presented in Ref. 33. For the 2nd equality, since $g(t, t')$ vanish when $t$ or $t' \rightarrow \pm\infty$, using integration by parts, we can show that converting a left/right derivative to another with an negative sign keeps the self-energy unchanged as a distribution. And Fourier transform of either form results in $\Sigma_\alpha^r(E) = [ES_{D\alpha} - h_{D\alpha}] g_\alpha^r(E) [ES_{\alpha D} - h_{\alpha D}]$.

We then follow the common assumption that the time-dependent bias voltage $\Delta_\alpha(t)$ only causes a rigid homogeneous shift to the potential in the lead region as well as near the lead-device interface. In this case, the transient self-energy is simply the ground/equilibrium self-energy picking up a time-dependent phase factor $\exp[i \int_{t'}^{t} d\tau \Delta_\alpha(\tau)]$ (see Appendix B for details),

$$\Sigma_\alpha^{<,>}(t, t') = \Sigma_\alpha^{<,>}(t - t')e^{i \int_{t'}^{t} d\tau \Delta_\alpha(\tau)}, \qquad (7)$$

where $\Sigma_\alpha^{<,>}(t - t')$ is the ground/equilibrium self-energy which depends only on the time difference $t - t'$. We define the energy-resolved self-energy as

$$\Sigma_\alpha^{<,>}(\epsilon, t, t') = \Sigma_\alpha^{<,>}(\epsilon)e^{i\epsilon(t-t')}e^{i \int_{t'}^{t} d\tau \Delta_\alpha(\tau)}, \qquad (8)$$

which follows the same equation of motion as in orthogonal basis:

$$i\frac{\partial}{\partial t}\Sigma_\alpha^{<,>}(\epsilon, t, t') = [\epsilon + \Delta_\alpha(t)]\Sigma_\alpha^{<,>}(\epsilon, t, t'). \qquad (9)$$

After deriving the equation of motion for energy-resolved lesser/greater self-energy, we now turn to the retarded/advanced self-energy. We would like to relate them to the broadening matrix $\Lambda_\alpha(t, t') = i\left[\Sigma_\alpha^>(t, t') - \Sigma_\alpha^<(t, t')\right]$, of which the equation of motion is known.

By putting $g_\alpha^r(t, t') = \theta(t - t')\left[g_\alpha^>(t, t') - g_\alpha^<(t, t')\right]$ into the expression of $\Sigma_\alpha^{r/a}(t, t')$ in Eq. (6) and after some rearrangement, we obtain

$$\Sigma_\alpha^r(t, t') = \delta(t - t')\Sigma_\alpha^\delta(t, t') + \delta^{(1)}(t - t')\Sigma_\alpha^{\delta'}(t, t') \\ - i\theta(t - t')\Lambda_\alpha(t, t'), \qquad (10)$$

where $\delta(t - t')$ is the Dirac delta function, $\delta^{(1)}(t - t')$ is the distributional derivative of delta function, and $\theta(t - t')$ is the Heaviside step function which is equal to one for any $t > t'$ and otherwise zero. $\Sigma^\delta(t, t')$, $\Sigma^{\delta'}(t, t')$ are defined as

$$\Sigma_\alpha^\delta(t, t') = -S_{D\alpha}A_\alpha(t, t')h_{\alpha D}(t') - h_{D\alpha}(t)A_\alpha(t, t')S_{\alpha D} \\ + 2iS_{D\alpha}\frac{\partial}{\partial t}A_\alpha(t, t')S_{\alpha D},$$

$$\Sigma_\alpha^{\delta'}(t, t') = iS_{D\alpha}A_\alpha(t, t')S_{\alpha D}, \qquad (11)$$

$$A_\alpha(t, t') = i\left[g_\alpha^>(t, t') - g_\alpha^<(t, t')\right].$$

It is noted that the first two terms in the right hand side of Eq. (10) are present only when there is a non-zero lead-device overlap $S_{D\alpha}$. In orthogonal basis, retarded self-energy simply satisfies $\Sigma_\alpha^r(t, t') = -i\theta(t - t')\Lambda_\alpha(t, t')$. These two terms appear due to the presence of time derivatives in expression of

self-energy in Eq. (6). When we apply time derivative on the Heaviside step function $\theta(t - t')$, a Dirac delta function comes out and a further derivative on $\delta(t - t')$ results in $\delta^{(1)}(t - t')$. And the presence of these two terms lead to a more generalized form of Kramer Kronig relation for the retarded self-energy in energy domain (see Appendix C for details).

From now on, we denote $\tilde{\Sigma}_\alpha^r(t, t') = -i\theta(t - t')\Lambda_\alpha(t, t')$, which behaves ordinarily as the retarded self-energy in orthogonal basis. Then, we put Eq. (10) into Eq. (5) to obtain the equation of motion for $G_D^<(t, t')$ in terms of $\tilde{\Sigma}_\alpha^r(t, t')$. Rearrange, we have

$$i\tilde{S}_D\frac{\partial}{\partial t}G_D^<(t, t') = \tilde{h}_D G_D^<(t, t') \\ + \sum_\alpha \int_{-\infty}^{\infty} d\tau \left[\tilde{\Sigma}_\alpha^r(t, \tau)G_D^<(\tau, t') \\ + \tilde{\Sigma}_\alpha^<(t, \tau)G_D^a(\tau, t')\right]. \qquad (12)$$

The tilde quantities are defined by

$$\tilde{S}_D = S_D - \sum_\alpha \Sigma_\alpha^1,$$

$$\tilde{h}_D(t) = h_D(t) + \sum_\alpha \Sigma_\alpha^0(t), \qquad (13)$$

$$\tilde{\Sigma}_\alpha^{r,a}(t, t') = \pm i\theta(\pm t \mp t')\Lambda_\alpha(t, t'),$$

$$\tilde{\Sigma}_\alpha^{<,>}(t, t') = \Sigma_\alpha^{<,>}(t, t'),$$

where $\Sigma_\alpha^0(t)$ and $\Sigma_\alpha^1$ are

$$\Sigma_\alpha^0(t) = S_{D\alpha}S_\alpha^{-1}h_\alpha(t)S_\alpha^{-1}S_{\alpha D} \\ - S_{D\alpha}S_\alpha^{-1}h_{\alpha D}(t) - h_{D\alpha}(t)S_\alpha^{-1}S_{\alpha D},$$

$$\Sigma_\alpha^1 = S_{D\alpha}S_\alpha^{-1}S_{\alpha D}. \qquad (14)$$

The equation of motion for $G_D^<(t, t')$ in non-orthogonal basis, taken into account the lead-device overlap, looks almost the same except that the overlap matrix, Fock matrix, and self-energies are replaced by the "effective" ones. It is worth noting that $\tilde{S}_D^{-1}$ is indeed the DD-block (the diagonal block corresponding to the device region) of the inverse of overlap matrix of the whole infinite system:

$$\tilde{S}_D^{-1} = \left(S_D - \sum_\alpha S_{D\alpha}S_\alpha^{-1}S_{\alpha D}\right)^{-1} = \left(S^{-1}\right)_{DD}. \qquad (15)$$

Thus $\Sigma_\alpha^1$ is like a "self-energy" for the overlap matrix added to ensure the same anti-commutation relation in device region: $\{a^i, a^{j\dagger}\} = (S^{-1})_{ij} = (\tilde{S}_D^{-1})_{ij}$ for $i, j \in D$. In practice, numerical calculation of $\Sigma_\alpha^0(t)$ and $\Sigma_\alpha^1$ is not an easy task and the details will be discussed in Appendix C.

Equations (9) and (12) are the central equations for deriving RSDM based HEOM in non-orthogonal basis. Plugging them into $i\dot{\sigma}_D(t) = \left[\frac{\partial}{\partial t}G_D^<(t, t') + \frac{\partial}{\partial t'}G_D^<(t, t')\right]\Big|_{t=t'}$, the RSDM based HEOM in non-orthogonal basis are then

obtained,

$$i\tilde{S}_D\dot{\sigma}_D(t)\tilde{S}_D = \tilde{h}_D(t)\sigma_D(t)\tilde{S}_D - \tilde{S}_D\sigma_D(t)\tilde{h}_D(t)$$
$$- \sum_\alpha \left(\tilde{S}_D\varphi_\alpha(t) - \varphi_\alpha^\dagger(t)\tilde{S}_D\right), \quad (16)$$

$$i\tilde{S}_D\dot{\varphi}_\alpha(\epsilon,t) = [\tilde{h}_D(t) - \tilde{S}_D(\epsilon+\Delta_\alpha)]\varphi_\alpha(\epsilon,t)$$
$$+ [f_\alpha(\epsilon) - \tilde{S}_D\sigma_D(t)]\Lambda_\alpha(\epsilon)$$
$$+ \sum_{\alpha'}\int d\epsilon' \, \varphi_{\alpha,\alpha'}(\epsilon,\epsilon',t), \quad (17)$$

$$i\dot{\varphi}_{\alpha,\alpha'}(\epsilon,\epsilon',t) = \left[\epsilon'+\Delta_{\alpha'}(t)-\epsilon-\Delta_\alpha(t)\right]\varphi_{\alpha,\alpha'}(\epsilon,\epsilon',t)$$
$$+\Lambda_{\alpha'}(\epsilon')\varphi_\alpha(\epsilon,t)-\varphi_{\alpha'}^\dagger(\epsilon',t)\Lambda_\alpha(\epsilon), \quad (18)$$

where $f_\alpha(\epsilon) = f(\epsilon-\mu_\alpha)$ is the Fermi distribution in lead $\alpha$ in equilibrium. $\varphi_\alpha(\epsilon,t)$ and $\varphi_{\alpha,\alpha'}(\epsilon,\epsilon',t)$ are the 1$^{\text{st}}$ and 2$^{\text{nd}}$ tier auxiliary reduced single-electron density matrices (AR-SDM) which are defined as follows. It is noted that in terms of lesser/greater self-energies, the definition of the ARSDM, Eqs. (20) and (22), is exactly the same as their definition in orthogonal basis:

$$\varphi_\alpha(\epsilon,t) = -i\left[\int_C d\tau\, G_D(t,\tau)\tilde{\Sigma}_\alpha(\epsilon;\tau,t)\right]^< \quad (19)$$

$$= i\int_{-\infty}^t d\tau\left[G_D^<(t,\tau)\Sigma_\alpha^>(\epsilon;\tau,t) - G_D^>(t,\tau)\Sigma_\alpha^<(\epsilon;\tau,t)\right], \quad (20)$$

$$\varphi_{\alpha,\alpha'}(\epsilon,\epsilon',t) = -i\left[\int_C d\tau_1\int_C d\tau_2\,\tilde{\Sigma}_{\alpha'}(\epsilon';t,\tau_1)G_D(\tau_1,\tau_2)\tilde{\Sigma}_\alpha(\epsilon;\tau_2,t)\right]^< \quad (21)$$

$$= i\int_{-\infty}^t d\tau_1\int_{-\infty}^t d\tau_2\left[\Sigma_{\alpha'}^>(\epsilon';t,\tau_1)-\Sigma_{\alpha'}^<(\epsilon';t,\tau_1)\right]\left[G_D^<(\tau_1,\tau_2)\Sigma_\alpha^>(\epsilon;\tau_2,t)-G_D^>(\tau_1,\tau_2)\Sigma_\alpha^<(\epsilon;\tau_2,t)\right]$$
$$+ i\int_{-\infty}^t d\tau_1\int_{-\infty}^t d\tau_2\left[\Sigma_{\alpha'}^<(\epsilon';t,\tau_1)G_D^a(\tau_1,\tau_2)\Sigma_\alpha^>(\epsilon;\tau_2,t)-\Sigma_{\alpha'}^>(\epsilon';t,\tau_1)G_D^a(\tau_1,\tau_2)\Sigma_\alpha^<(\epsilon;\tau_2,t)\right]. \quad (22)$$

## B. An alternative way: Lead-device orthogonalization

In this section, we will show that the above result can be obtained in another way: by a block diagonalization of the overlap matrix. We start by seeking a basis transformation $\tilde{\chi} = U\chi$ upon which the overlap between basis in device and lead regions vanishes, i.e., $\tilde{S}_{D\alpha} = \tilde{S}_{\alpha D} = 0$, while keeping the basis $\{\chi_L, \chi_R\}$ in lead region unchanged so that the locality of basis as well as periodicity in lead region is preserved:

$$\tilde{\chi} = \begin{bmatrix}\chi_L\\\tilde{\chi}_D\\\chi_R\end{bmatrix} = \begin{bmatrix}I & 0 & 0\\U_{DL} & U_{DD} & U_{DR}\\0 & 0 & I\end{bmatrix}\begin{bmatrix}\chi_L\\\chi_D\\\chi_R\end{bmatrix}, \quad (23)$$

$$\tilde{S} = USU^T = \begin{bmatrix}S_L & 0 & 0\\0 & \tilde{S}_D & 0\\0 & 0 & S_R\end{bmatrix},$$
$$\tilde{h} = UhU^T = \begin{bmatrix}h_L & \tilde{h}_{LD} & 0\\\tilde{h}_{DL} & \tilde{h}_D & \tilde{h}_{DR}\\0 & \tilde{h}_{RD} & h_R\end{bmatrix}. \quad (24)$$

There are many kinds of transformations which satisfy this requirement, one of which has already been suggested by Thygesen utilizing the duel basis.[39] In that case, the transformation is given by $U_{DL} = (S^{-1})_{DL}, U_{DD} = (S^{-1})_{DD}, U_{DR} = (S^{-1})_{DR}$ such that the device region is now expanded by the duel basis. Here, we will choose another one by setting

$U_{DD} = I$. After some linear algebra, we find

$$U = \begin{bmatrix}I & 0 & 0\\-S_{DL}S_L^{-1} & I & -S_{DR}S_R^{-1}\\0 & 0 & I\end{bmatrix}. \quad (25)$$

The transformed overlap and Fock matrices are

$$\tilde{S}_D = S_D - \sum_{\alpha=L,R} S_{D\alpha}S_\alpha^{-1}S_{\alpha D},$$
$$\tilde{h}_D = h_D + \sum_{\alpha=L,R}\left[S_{D\alpha}S_\alpha^{-1}h_\alpha S_\alpha^{-1}S_{\alpha D}\right.$$
$$\left. - S_{D\alpha}S_\alpha^{-1}h_{\alpha D} - S_{D\alpha}S_\alpha^{-1}h_{\alpha D}\right], \quad (26)$$
$$\tilde{h}_{D\alpha} = h_{D\alpha} - S_{D\alpha}S_\alpha^{-1}h_\alpha.$$

The transformed matrices $\tilde{S}_D$ and $\tilde{h}_D$ are exactly what we obtained in Sec. II A. (Therefore, we denote them with the same notation.) Also, since $h_\alpha$ remains unchanged, so does the surface Green's function and one can check that the retarded (or advanced) self-energy in the new basis is exactly the $\tilde{\Sigma}_\alpha^{r,a}$ in Sec. II A,

$$\tilde{\Sigma}_\alpha^{r,a}(E) = \tilde{h}_{D\alpha}g_\alpha^{r,a}(E)\tilde{h}_{\alpha D}$$
$$= \Sigma_\alpha^{r,a}(E) - \Sigma_\alpha^0 - \Sigma_\alpha^1 E. \quad (27)$$

Furthermore, the transformed RSDM $\tilde{\boldsymbol{\sigma}} = \boldsymbol{U}^{-T}\boldsymbol{\sigma}\boldsymbol{U}^{-1}$ (as well as the Green's functions) for the device region remains unchanged. This is a consequence of choosing $\boldsymbol{U}_{DD} = \boldsymbol{I}$ and this means that propagation of this transformed system results in exactly the same DD-block of RSDM and Green's functions

$$\tilde{\boldsymbol{\sigma}}_D = \boldsymbol{\sigma}_D, \tag{28}$$

$$\tilde{\boldsymbol{\sigma}}_{\alpha D} = \boldsymbol{\sigma}_{\alpha D} + \boldsymbol{S}_\alpha^{-1}\boldsymbol{S}_{\alpha D}\boldsymbol{\sigma}_D, \tag{29}$$

$$\tilde{\boldsymbol{\sigma}}_\alpha = \boldsymbol{\sigma}_\alpha + \boldsymbol{\sigma}_{\alpha D}\boldsymbol{S}_{D\alpha}\boldsymbol{S}_\alpha^{-1} + \boldsymbol{S}_\alpha^{-1}\boldsymbol{S}_{\alpha D}\boldsymbol{\sigma}_{D\alpha}$$
$$+\boldsymbol{S}_\alpha^{-1}\boldsymbol{S}_{\alpha D}\boldsymbol{\sigma}_D\boldsymbol{S}_{D\alpha}\boldsymbol{S}_\alpha^{-1}. \tag{30}$$

We can then derive the HEOM of $\boldsymbol{\sigma}_D(t)$ in this transformed basis, which is straightforward because this can be done without having to take into account the lead-device basis overlap. The resulting HEOM are exactly the same as the HEOM we derived in Sec. II A (Eqs. (16)–(18)). This means that our previous approach to include the lead-device basis overlap into the self-energy is equivalent to this lead-device orthogonalization. Of course, we will not carry out this lead-device orthogonalization in practice since the matrices are infinite in size. Instead, we propagate the HEOM derived in Sec. II A.

## C. Time-dependent current

The particle current passing through the lead-device interface can be defined by the derivative of number of electrons in lead region $J_\alpha(t) = -e\frac{d}{dt}N_\alpha(t)$, where $e$ is the electron charge. However, in non-orthogonal basis, there is ambiguity in defining the number of electrons $N_\alpha(t)$ in each subspaces due to the lead-device overlap and this has been discussed by Viljas *et al.*[37] This is similar to the problem of assigning bonding electrons to individual atoms in Mulliken population analysis. Here, we start by defining $N_\alpha(t)$ as the integral of density over the real space belonging to the lead $\alpha$ and derive the transient current formula in terms of the RSDM,

$$N_\alpha(t) = \int_{\vec{r}\in\alpha} dr^3 \rho(\vec{r}, t)$$

$$= \sum_{i,j} \sigma_{ij}(t) \int_{\vec{r}\in\alpha} dr^3 \chi_j^*(\vec{r})\chi_i(\vec{r})$$

$$\approx tr\left[\boldsymbol{\sigma}_\alpha(t)\boldsymbol{S}_\alpha\right] + \frac{1}{2}tr\left[\boldsymbol{\sigma}_{\alpha D}(t)\boldsymbol{S}_{D\alpha} + \boldsymbol{\sigma}_{D\alpha}(t)\boldsymbol{S}_{\alpha D}\right]$$

$$= tr\left[\boldsymbol{\sigma}_\alpha(t)\boldsymbol{S}_\alpha\right] + \text{Re}\left[tr\left[\boldsymbol{\sigma}_{\alpha D}(t)\boldsymbol{S}_{D\alpha}\right]\right]. \tag{31}$$

The third step utilizes the locality of basis and equipartitions the off-diagonal density to lead and device regions. The equipartition is justified by the fact that we include part of the electrodes into the device region (recall Fig. 1),

$$\sum_{i,j\in D} \sigma_{ij}(t) \int_{\vec{r}\in\alpha} dr^3 \chi_j^*(r)\chi_i(r) \approx 0, \tag{32}$$

$$\sum_{k\in\alpha, j\in D} \sigma_{kj}(t) \int_{\vec{r}\in\alpha} dr^3 \chi_j^*(r)\chi_k(r)$$

$$\approx \sum_{k\in\alpha, j\in D} \sigma_{kj}(t) \int_{\vec{r}\in D} dr^3 \chi_j^*(r)\chi_k(r)$$

$$\approx \frac{1}{2}tr\left[\boldsymbol{\sigma}_{\alpha D}(t)\boldsymbol{S}_{D\alpha}\right]. \tag{33}$$

From the equation of motion of RSDM in Eqs. (16)–(18), it can be shown that the trace of the 1$^{st}$ tier ARSDM counts the time-derivative of the number of electrons in the lead in the transformed basis, i.e., $2\,tr\left[\text{Im}\boldsymbol{\varphi}_\alpha(t)\right] = tr\left[\frac{d}{dt}\tilde{\boldsymbol{\sigma}}_{\alpha\alpha}(t)\boldsymbol{S}_{\alpha\alpha}\right]$. With Eq. (30), we can show that the transient current is given by

$$J_\alpha(t) = -e\,tr\left[2\text{Im}\boldsymbol{\varphi}_\alpha(t) - \text{Re}\dot{\boldsymbol{\sigma}}_{\alpha D}(t)\boldsymbol{S}_{D\alpha} - \dot{\boldsymbol{\sigma}}_D(t)\boldsymbol{\Sigma}_\alpha^1\right]. \tag{34}$$

The only problem here is that we do not know what $\boldsymbol{\sigma}_{\alpha D}(t)$ are ($\alpha = L, R$). Following their time evolution is difficult and computationally expensive because they are in principle matrices of infinite size. However, since the term $tr[\text{Re}\boldsymbol{\sigma}_{\alpha D}(t)\boldsymbol{S}_{D\alpha}]$ corresponds to the bonding electrons near the lead-device interface, its contribution to the current should be insignificant. Otherwise, there will be a change in the chemical bonds inside the electrodes, which are assumed to be always in equilibrium. Therefore, in practical calculation, one may simply neglect this term. But here, in our implementation, we try to approximate this term by including at least two principal layers of the electrodes in the device region so that we can approximate $\boldsymbol{\sigma}_{LD}(t)$ and $\boldsymbol{\sigma}_{RD}(t)$ by the first and last off-diagonal block of $\boldsymbol{\sigma}_D(t)$, respectively, i.e.,

$$\sigma_{k_L,i}(t) \approx \sigma_{k_L+N_L,i+N_L}(t), \tag{35}$$

$$\sigma_{k_R,i}(t) \approx \sigma_{k_R-N_R,i-N_R}(t), \tag{36}$$

where $N_{L/R}$ are the number of orbitals in a principal layer of the left/right lead, $k_{L/R} \in L/R$ and $i, i \pm N_{L/R}, k_{L/R} \pm N_{L/R} \in D$.

Although the transient current formula in non-orthogonal basis in Eq. (34) looks complex, it is clear that the current formula reduces to the Landauer formula in the steady state limit because both $\dot{\boldsymbol{\sigma}}_{\alpha D}(t)$ and $\dot{\boldsymbol{\sigma}}_D(t)$ equal to zero in steady state due to the translational invariance in time. The Landauer formula can then be obtained by Fourier transforming Eq. (20) to the energy-domain.

## III. NUMERICAL IMPLEMENTATION

We implemented the above TDDFT-NEGF-HEOM formalism with the Lorentzian-Padè decomposition scheme.[23] Under this scheme, we approximate the broadening matrix $\Lambda_\alpha(\epsilon)$ by a bunch of Lorentzian functions and the Fermi-Dirac distribution by Padè spectrum decomposition.[41] Padè spectrum decomposition serves as an efficient way to decompose the Fermi distribution in numerical implementation so that the number of energy-resolved self-energy is minimized. It has been shown that Padè spectrum decomposition converges much faster than other schemes such as Matsubara

expansion,[41]

$$\mathbf{\Lambda}_\alpha(\epsilon) \approx \sum_{d=1}^{N_d} \frac{w_d{}^2}{(\epsilon - \Omega_d)^2 + w_d{}^2} \bar{\mathbf{\Lambda}}_{\alpha,d}, \qquad (37)$$

$$f(\epsilon - \mu) \approx \frac{1}{2} - \sum_p \left( \frac{R_p}{\epsilon - \mu + i z_p} + \frac{R_p}{\epsilon - \mu - i z_p} \right). \qquad (38)$$

The lesser/greater self-energy $\mathbf{\Sigma}_\alpha^{<,>}(t,t')$ can then be written as a summation form by residue theorem. For $t < t'$, it is a summation of residues in the upper half complex plane. For $t > t'$, it is a summation of residues in the lower half complex plane,

$$\mathbf{\Sigma}_\alpha^{<,>}(t,t') = \frac{i}{2\pi} \int_{-\infty}^{\infty} d\epsilon \, f_\alpha^{<,>}(\epsilon) \Lambda_\alpha(\epsilon) e^{i\epsilon(t'-t)} e^{i \int_t^{t'} d\tau \, \Delta_\alpha(\tau)},$$

$$= \begin{cases} \sum_k \mathbf{A}_{\alpha,k}^{<,>+} e^{i\epsilon_{\alpha,k}(t'-t)} e^{i \int_t^{t'} d\tau \, \Delta_\alpha(\tau)} & (t < t') \\ \sum_k \mathbf{A}_{\alpha,k}^{<,>-} e^{i\epsilon_{\alpha,k}^*(t'-t)} e^{i \int_t^{t'} d\tau \, \Delta_\alpha(\tau)} & (t > t') \end{cases}, \qquad (39)$$

where $f_\alpha^<(\epsilon) = f_\alpha(\epsilon)$ is the Fermi-Dirac distribution for lead $\alpha$, $f_\alpha^>(\epsilon) = 1 - f_\alpha(\epsilon)$, $\epsilon_{\alpha,k}$ are the poles of $\Lambda_\alpha(\epsilon)$ and $f_\alpha^{<,>}(\epsilon)$ on the upper half complex plane. $\epsilon_{\alpha,k}^*$ are the complex conjugate of $\epsilon_{\alpha,k}$, the poles on the lower half complex plane. For poles of $\Lambda_\alpha(\epsilon)$,

$$\epsilon_{\alpha,d} = \Omega_d + i W_d,$$
$$\mathbf{A}_{\alpha,d}^{<,>+} = \pm i \frac{w_d}{2} \bar{\Lambda}_{\alpha,d} f^{<,>}(\epsilon_{\alpha,d} - \mu_\alpha), \qquad (40)$$
$$\mathbf{A}_{\alpha,d}^{<,>-} = \pm i \frac{w_d}{2} \bar{\Lambda}_{\alpha,d} f^{<,>}(\epsilon_{\alpha,d}^* - \mu_\alpha).$$

For poles of $f_\alpha^{<,>}(\epsilon)$,

$$\epsilon_{\alpha,p} = \mu_\alpha + i z_p,$$
$$\mathbf{A}_{\alpha,p}^{<,>+} = R_p \Lambda_\alpha(\epsilon_{\alpha,p}), \qquad (41)$$
$$\mathbf{A}_{\alpha,p}^{<,>-} = R_p \Lambda_\alpha(\epsilon_{\alpha,p}^*).$$

The energy-resolved self-energy can then be redefined as: $\mathbf{\Sigma}_{\alpha,k}^{<,>}(t,t') = \mathbf{A}_{\alpha,k}^{<,>\pm} e^{i\epsilon_{\alpha,k}(t'-t)} e^{i \int_t^{t'} d\tau \, \Delta_\alpha(\tau)}$, where $\pm$ depends on whether $t < t'$ or $t > t'$. And we can then rewrite the energy-integral in HEOM (Eqs. (16)–(18)) into a summation form,

$$i\tilde{\mathbf{S}}_D \dot{\mathbf{\sigma}}_D(t) \tilde{\mathbf{S}}_D = \tilde{\mathbf{h}}_D(t) \mathbf{\sigma}_D(t) \tilde{\mathbf{S}}_D - \tilde{\mathbf{S}}_D \mathbf{\sigma}_D(t) \tilde{\mathbf{h}}_D(t)$$
$$- \sum_{\alpha,k} (\tilde{\mathbf{S}}_D \mathbf{\varphi}_{\alpha,k}(t) - \mathbf{\varphi}_{\alpha,k}^\dagger(t) \tilde{\mathbf{S}}_D),$$

$$i\tilde{\mathbf{S}}_D \dot{\mathbf{\varphi}}_{\alpha,k}(t) = [\tilde{\mathbf{h}}_D(t) - \tilde{\mathbf{S}}_D(\epsilon_{\alpha,k} + \Delta_\alpha(t))] \mathbf{\varphi}_{\alpha,k}(t)$$
$$- [i\mathbf{A}_{\alpha,k}^{<+} + \tilde{\mathbf{S}}_D \mathbf{\sigma}_D \mathbf{\Lambda}_{\alpha,k}]$$
$$+ \sum_{\alpha'k'} \mathbf{\varphi}_{\alpha k,\alpha'k'}(t), \qquad (42)$$

$$i\dot{\mathbf{\varphi}}_{\alpha k,\alpha'k'}(t) = [\epsilon_{\alpha',k'}^* + \Delta_{\alpha'}(t) - \epsilon_{\alpha,k} - \Delta_\alpha(t)] \mathbf{\varphi}_{\alpha k,\alpha'k'}(t)$$
$$+ \mathbf{\Lambda}_{\alpha',k'} \mathbf{\varphi}_{\alpha,k}(t) - \mathbf{\varphi}_{\alpha',k'}^\dagger(t) \mathbf{\Lambda}_{\alpha,k},$$

where $\mathbf{\Lambda}_{\alpha,k} = i[\mathbf{A}_{\alpha,k}^{>+} - \mathbf{A}_{\alpha,k}^{<+}] = i[\mathbf{A}_{\alpha,k}^{>-} - \mathbf{A}_{\alpha,k}^{<-}]$.

Our numerical implementation is then simple.

1.  The equilibrium Kohn-Sham Fock matrix is obtained by self-consistent field calculation.
2.  Retarded self-energy $\mathbf{\Sigma}_\alpha^r(E)$ is calculated and its imaginary part is expanded with Lorentzian functions by least square regression.
3.  Initial values (equilibrium values) of $\mathbf{\sigma}_D, \mathbf{\varphi}_{\alpha,k}$ and $\mathbf{\varphi}_{\alpha k,\alpha'k'}$ are solved by NEGF techniques.
4.  Runge-Kutta 4th order method is used to propagate the HEOM in Eqs. (42). Current $J_\alpha(t)$ is evaluated using Eq. (34).

Technical details including calculation of $\tilde{\mathbf{S}}_D$, $\tilde{\mathbf{h}}_D(t)$ and the initial values are discussed in Appendices C and D.

## IV. RESULTS

To demonstrate our method, we simulated two simple system: a one-dimensional carbon chain and a carbon chain-benzene-carbon chain (C-benzene-C) system as shown in Fig. 2. The linear C-chain system is simulated at TDDFT level while the C-benzene-C system is simulated at density functional tight-binding (DFTB) level, which is an approximated DFT method derived from the second-order expansion of DFT Kohn-Sham energy respect to charge density fluctuation.[42,43] These two systems are both connected to carbon chain electrodes but differ in the device region. And while results can be shown for both systems with both methods, here we only show TDDFT results for the first system and DFTB results for the second one for demonstration purpose. For TDDFT simulation, the minimal basis set STO-3G is used and adiabatic local-density approximation[44] is adopted as the XC functional. The electronic temperature is set at 300 K and 50 terms are used in Padè decomposition of Fermi-Dirac distribution to achieve an accuracy of $10^{-7}$ within the energy range $[\mu - 32\,\text{eV}, \mu + 32\,\text{eV}]$. The system is initially in the equilibrium state and a time-dependent bias voltage is applied, driving the system out of equilibrium.

We apply least square regression to fit $\mathbf{\Lambda}_\alpha(E)$ of the carbon chain electrode with a total number of 63 Lorentzian functions. Figure 3 shows the accurate and fitted self-energies. The real part of fitted $\mathbf{\Sigma}_\alpha^r(E)$ is calculated with Eq. (C5) in Appendix C. We can see a good agreement between the accurate and fitted self-energies, showing the applicability of Lorentzian expansion. Figure 4 shows the transmission coefficient of (top) linear C-chain and (bottom) C-benzene-C system at equilibrium calculated exactly with standard NEGF techniques, with self-energies fitted with Lorentzian functions and with the WBL approximation.[45] To show the details near Fermi level clearly, we replot the graphs with enlarged energy
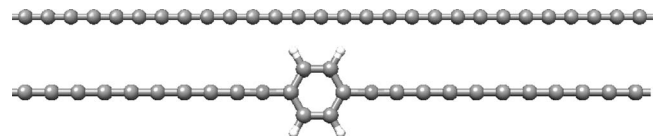


FIG. 2. Structure of (top) linear C-chain and (bottom) C-benzene-C system. The C–C bond length and C–H bond length are 1.42 Å and 1.08 Å, respectively.
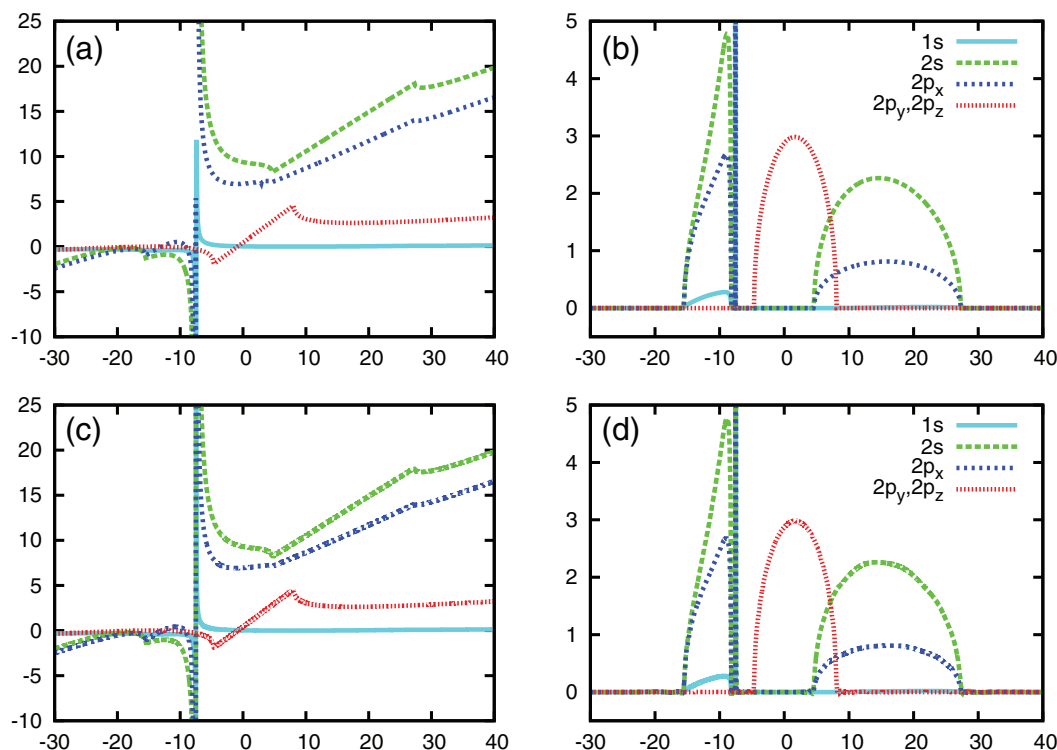
FIG. 3.  Accurate and fitted retarded self-energy. For simplicity, only the first five diagonal elements (corresponding to the 1$s$, 2$s$, 2$p_x$, 2$p_y$, and 2$p_z$ orbitals of the first carbon atom) are shown. Top two figures show the (a) real part and (b) imaginary part of the accurate retarded self-energy $\Sigma_\alpha^r(E)$ against $E$ (in the unit of eV). Similarly, bottom figures are the self-energy approximated by a sum of Lorentzian functions.

scale and they are shown in the right panel. Again, the exact and fitting results coincide very well. For the WBL case, the self-energies are assumed to be independent of energy, with their values taken at the Fermi level, i.e., $\Sigma_\alpha^r(E) = \Sigma_\alpha^r(\mu_\alpha)$. The transmission spectra calculated with WBL are more oscillatory and they are only accurate within a certain energy range near the Fermi level.

### A.  Linear carbon chain

Figure 5 shows the time-dependent current through the C-chain under source-drain voltage 1 V, 2 V, and 4 V. The voltage is switched on exponentially $\Delta_{R,L} = \pm V_0(1 - e^{-t/\tau})$, where $\tau$ is fixed at 1 fs. The blue solid curves are calculated using HEOM approach with Lorentzian Padè
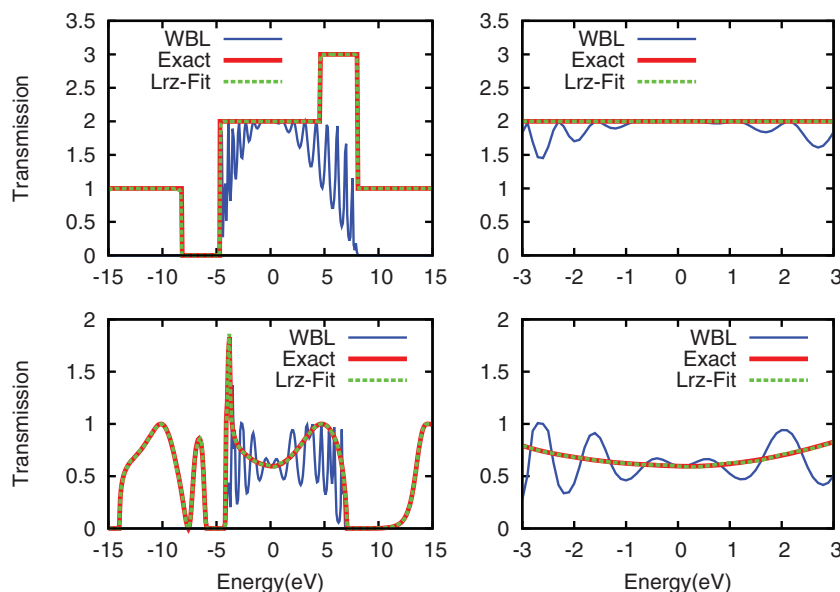


FIG. 4.  Transmission coefficient for C-chain (top panel) and C-benzene-C (bottom panel) system at V = 0. (Red: transmission calculated exactly; green: with Lorentzian-fitted self-energy; and blue: with WBL approximation.) Right panel shows the plot with enlarged energy scale.
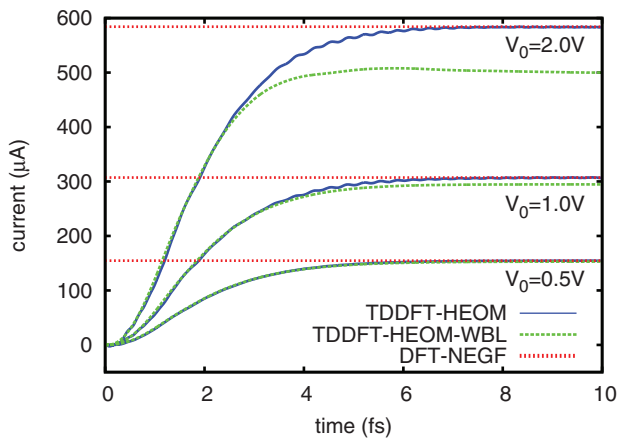
FIG. 5. Time-dependent current through the right lead $J_R(t)$ in the linear C-chain system. The voltage applied is $\Delta_{R,L} = \pm V_0(1 - e^{-t/\tau})$, where $\tau = 1$ fs, $V_0 = 0.5$ V, 1 V, and 2 V.



FIG. 7. Time-dependent current through the right lead $J_R(t)$ in the C-benzene-C system. The voltage applied is $\Delta_{R,L} = \pm V_0(1 - e^{-t/\tau})$, where $\tau = 0.1$ fs, $V_0 = 0.5$ V, 1 V, and 2 V.

decomposition scheme presented in this article. The green dashed curves are calculated using HEOM approach with the WBL approximation.[22] The red dotted horizontal lines are the steady state current calculated by Landauer formula from non-WBL self-consistent calculation. The good agreement between the steady state currents obtained from self-consistent calculation (dotted curves) and time-dependent simulation (solid curves) validates the correctness of our method and verifies our scheme as beyond the WBL.

Figure 6 presents the transient current when we switch on the voltage with different time constant $\tau$, with the final source-drain voltage fixed at 1 V. Again, comparison with WBL calculation is made. It can be seen that the non-WBL and WBL calculations agree well when the voltage is switched on slowly. For fast switch-on, non-WBL calculation gives more oscillatory transient current. This is because the time-dependent self-energies in non-WBL calculation consist of many components oscillating with different frequencies (Eq. (39)). For the case where $V_0 = 0.5$ V and $\tau = 0.1$ fs, we also checked the time-dependent current contributed from the term $tr[\text{Re}\dot{\boldsymbol{\sigma}}_{\alpha D}(t)\boldsymbol{S}_{D\alpha}]$, which is approximated by the method discussed in Sec. II C. Its contribution never exceeds 0.3 $\mu$A throughout the simulation and is thus negligible.

## B. C-benzene-C system

For the C-benzene-C system, the device region consists of the benzene ring together with 11 carbons of the carbon chain on each side. This time, the simulation is done at DFTB level. Figure 7 shows the time-dependent current at different voltage. Again, good agreement is obtained between non-WBL HEOM and self-consistent steady state calculation. Figure 8 shows the time-dependent current through our system given a time-dependent voltage in sinusoidal form. In both figures, the time-dependent current under WBL approximation agrees pretty well with the non-WBL results qualitatively even under large voltage or high frequency ac voltage. This indicates that the linear C-chain electrode behaves very well as a wide-band conductor.

## V. COMPUTATIONAL COMPLEXITY

The computational complexities of propagating different tiers of the HEOM are different. Consider a typical two-terminal system, one can order the orbitals in a way that the
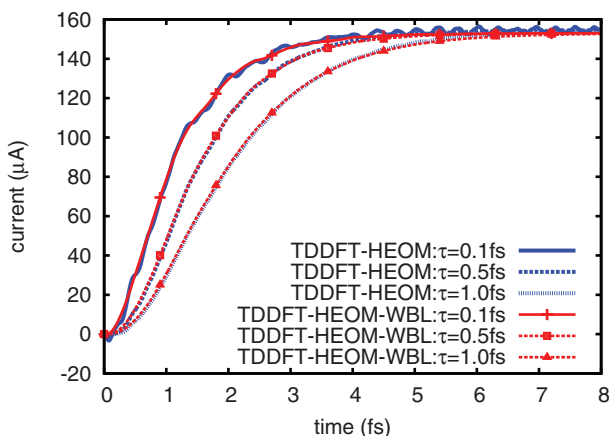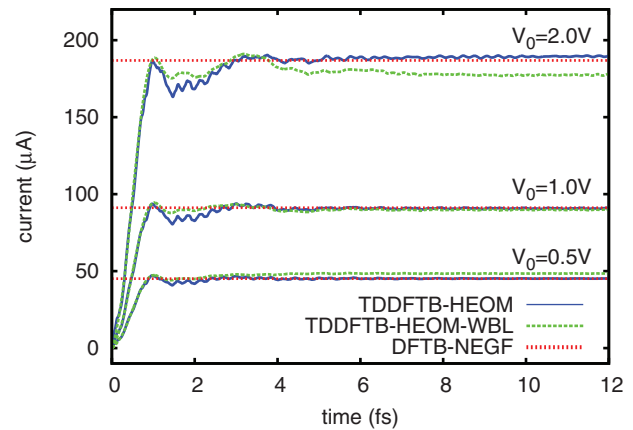


FIG. 6. Time-dependent current through the right lead $J_R(t)$ in the linear C-chain system. The voltage applied is $\Delta_{R,L} = \pm V_0(1 - e^{-t/\tau})$, where $V_0 = 0.5$ V, $\tau = 0.1$ fs, 0.5 fs, and 1.0 fs.
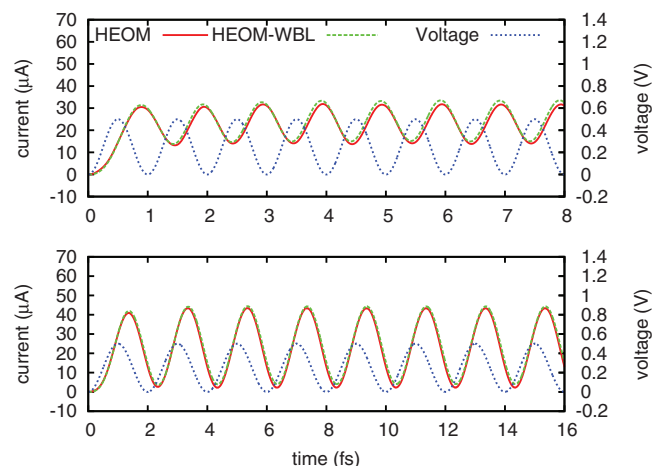


FIG. 8. Time-dependent current through the right lead $J_R(t)$ in the C-benzene-C system. The voltage applied is $\Delta_R(t) = -\Delta_L(t) = V_0(1 - \cos(2\pi t/T))$, where $V_0 = 0.5$ V, $T = 1$ fs (top) and 2 fs (bottom), respectively. The blue dotted curves correspond to voltage on the right lead $V_R(t)$.
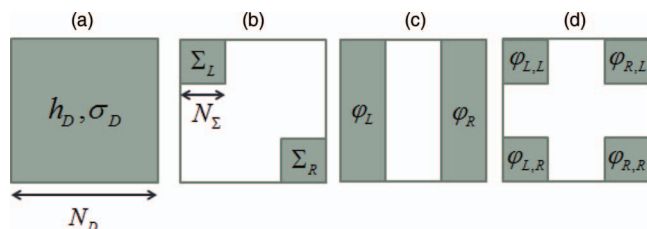
FIG. 9. Locality of the matrices: (a) $\boldsymbol{h}_D(t), \boldsymbol{\sigma}_D(t)$; (b) self-energies $\boldsymbol{\Sigma}_\alpha$; (c) 1$^{\text{st}}$ tier ARSDM $\boldsymbol{\varphi}_\alpha(t)$; and (d) 2$^{\text{nd}}$ tier ARSDM $\boldsymbol{\varphi}_{\alpha,\alpha'}(t)$ for $\alpha, \alpha' \in \{L, R\}$.

self-energy due to lead-device coupling is localized on top-left or bottom-right corner. Let $\boldsymbol{\sigma}_D$, $\boldsymbol{h}_D$ be $N_D \times N_D$ matrices while the actual size of the self-energies are $N_\Sigma \times N_\Sigma$. The sizes of 1$^{\text{st}}$ tier and 2$^{\text{nd}}$ tier ARSDM are $N_D \times N_\Sigma$ and $N_\Sigma \times N_\Sigma$, respectively (shown in Fig. 9). This can be seen from their definitions in Eqs. (20) and (22). The locality of ARSDM keeps unchanged under time propagation, which can be checked from the HEOM.

As a result, the memory requirement for storing the RSDM and ARSDM is given by $O(N_D^2 + N_D N_\Sigma N_k + N_\Sigma^2 N_k^2)$, where $N_k$ is the number of poles in the Lorentzian-Padè decomposition scheme. And the computational complexities for propagating RSDM, 1$^{\text{st}}$ and 2$^{\text{nd}}$ tier ARSDM are $O(N_D^3)$, $O(N_k N_D^2 N_\Sigma)$, $O(N_k^2 N_\Sigma^3)$, respectively. The computational time for propagating the 2$^{\text{nd}}$ tier ARSDM depends only on $N_k$, $N_\Sigma$, which is determined by the nature of electrodes but not the device. Figure 10 shows computational time for propagating each tier of the HEOM for a single time step of the carbon chain in logarithmic scale. It can be seen that, for short devices, where $N_D \ll N_k N_\Sigma$, the computational time is dominated by the propagation of 2$^{\text{nd}}$ tier and is insensitive to the change of $N_D$. When the length of the device becomes long, where $N_D \gg N_k N_\Sigma$, propagation of RSDM dominates and it scales as $O(N_D^3)$.

Finally, we note that the localized structures of the AR-SDM come from the localized non-orthogonal atomic orbital basis we used. Orthogonalizing the basis would result in a denser Fock matrix and more delocalized ARSDM. But on the other hand, orthogonalizing the basis simplifies the equations of motion since the overlap matrix becomes a unity. Therefore, in terms of computational performance, there are
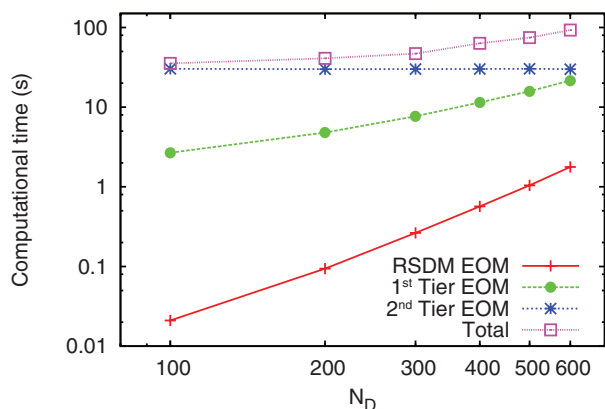
no clear advantages for orthogonalizing the system over using the non-orthogonal basis directly and vice versa.

## VI. SUMMARY

In this work, we extend the RSDM based HEOM formalism to the case of a non-orthogonal basis so that it is directly implementable with first principles TDDFT with non-orthogonal atomic orbital basis. The formalism is implemented with TDDFT as well as TDDFTB and simulation results are presented. The Lorentzian-Padè decomposition scheme, in which the linewidth matrix is fitted with multi-Lorentzian functions rather than an energy-independent constant, is applied to expand the time dependent self-energy as a sum of different frequency components. Therefore, it is a scheme beyond the WBL approximation. Good agreement is achieved between the transmission calculated with accurate and fitted self-energies, respectively, which confirms the feasibility of fitting the linewidth function with multi-Lorentzian functions. Simulations also show good agreement between the steady state current obtained by time-dependent simulation and self-consistent steady state calculation, which confirm the validity of our method. However, readers are reminded that reaching of steady state is not guaranteed in general. There are possibilities of existence of multiple steady states or dynamic steady state.[46–48] After validating our method, comparison with WBL approximation is then made. The WBL results agree well with the non-WBL results when the applied voltage is small and switched on slowly. For large voltage or fast switch on, the transient current in non-WBL calculation generally shows more oscillation.

Finally, the sparsity of the matrices is discussed and computational complexity for propagating the corresponding equations of motion are demonstrated. Compared with the RSDM based HEOM approach with WBL approximation which terminates at the 1$^{\text{st}}$ tier, the non-WBL HEOM require propagation of $N_\alpha^2 N_k^2$ 2$^{\text{nd}}$ tier ARSDM $\boldsymbol{\varphi}_{\alpha k, \alpha' k'}(t)$. Fortunately, the 2$^{\text{nd}}$ tier ARSDM are sparse matrices with actual size $N_\Sigma \times N_\Sigma$. Thus the computational cost and memory requirement due to the introduction of 2$^{\text{nd}}$ tier ARSDM are constant with respect to the length of the device. And with the Lorentzian-Padè decomposition scheme, the number of expansion $N_k$ only depends on temperature and the complexity of linewidth function. Thus the computational cost scales linearly with respect to the simulation time. So this RSDM based TDDFT-NEGF-HEOM approach is efficient in simulating the time-dependent response of realistic molecular devices.

FIG. 10. Computational time for propagating each tier of the HEOM for a single time step versus the size of device in logarithmic scale.

## APPENDIX A: MATRIX REPRESENTATION IN NON-ORTHOGONAL BASIS

In this section, we give a brief introduction on duel basis and matrix representations in non-orthogonal basis. Given any basis set $|\chi_\mu\rangle$, it is known that we can construct a unique duel basis $|\chi^\mu\rangle$ which fulfills

$$\langle \chi_\mu \mid \chi^\nu \rangle = \langle \chi^\mu \mid \chi_\nu \rangle = \delta_{\mu\nu}. \qquad (A1)$$

In particular, if $|\chi_\mu\rangle$ is a finite basis, its duel basis is given by

$$|\chi^\mu\rangle = \sum_\nu (S^{-1})_{\mu\nu} |\chi_\nu\rangle , \qquad (A2)$$

where $S_{\mu\nu} = \langle \chi_\mu \mid \chi_\nu \rangle$. And the completeness relation is written as

$$\sum_\mu |\chi_\mu\rangle\langle\chi^\mu| = \sum_{\mu\nu} |\chi_\mu\rangle(S^{-1})_{\mu\nu}\langle\chi_\nu| = I. \qquad (A3)$$

In non-orthogonal basis, there are three different ways to represent an operator by a matrix. They are given by

$$\begin{aligned} H_{\mu\nu} &= \langle\chi_\mu|\hat{H}|\chi_\nu\rangle, \\ H^{\mu\nu} &= \langle\chi^\mu|\hat{H}|\chi^\nu\rangle, \\ H^\mu_\nu &= \langle\chi^\mu|\hat{H}|\chi_\nu\rangle. \end{aligned} \qquad (A4)$$

They are known as the covariant, contravariant, and mixed representation, respectively. They are related to each other simply by the overlap matrix, for instance, $H_{\mu\nu} = \sum_{\delta\gamma} S_{\mu\delta} H^{\delta\gamma} S_{\gamma\nu}$. Therefore, they are equivalent in orthogonal basis. And one can show that they can be defined alternatively as

$$\begin{aligned} \hat{H} &= \sum_{\mu\nu} H_{\mu\nu}|\chi^\mu\rangle\langle\chi^\nu|, \\ \hat{H} &= \sum_{\mu\nu} H^{\mu\nu}|\chi_\mu\rangle\langle\chi_\nu|, \\ \hat{H}|\chi_\nu\rangle &= \sum_\mu H^\mu_\nu|\chi_\mu\rangle. \end{aligned} \qquad (A5)$$

Throughout this paper, contravariant representation is used for the RSDM and Green's function while covariant representation is used for all other operators. This is a natural choice because under this convention, the matrix elements of operators, e.g., $A_{\mu\nu} = \langle\chi_\mu| \hat{A} |\chi_\nu\rangle$, as well as their expectation values, e.g., $\langle A\rangle = tr\,[\boldsymbol{\sigma}\boldsymbol{A}]$, can be evaluated as usual.

In the language of second quantization, as we will see, it is more convenient to express the Green's function and other operators in terms of the creation and annihilation operator in duel basis $a^{\mu\dagger}$ ($a^\mu$) which creates (destroys) an electron in $|\chi^\mu\rangle$. They obey the anti-commutation relation

$$\{a^i, a^{j\dagger}\} = (S^{-1})_{ij}. \qquad (A6)$$

Any operator in covariant representation is then expressed as

$$\hat{h}(t) = \sum_{\mu\nu} h_{\mu\nu}(t)a^{\mu\dagger}a^\nu. \qquad (A7)$$

In Heisenberg picture, the creation and annihilation operators in duel basis are

$$\begin{aligned} a^\mu(t) &= e^{i\int_{t_0}^t d\tau H(\tau)}a^\mu e^{-i\int_{t_0}^t d\tau H(\tau)}, \\ a^{\mu\dagger}(t) &= e^{i\int_{t_0}^t d\tau H(\tau)}a^{\mu\dagger} e^{-i\int_{t_0}^t d\tau H(\tau)}. \end{aligned} \qquad (A8)$$

The retarded, advanced, lesser, and greater Green's function are then defined as

$$\begin{aligned} G^r_{\mu\nu}(t, t') &= -i\theta(t - t')\langle\{a^\mu(t), a^{\nu\dagger}(t')\}\rangle, \\ G^a_{\mu\nu}(t, t') &= i\theta(t' - t)\langle\{a^\mu(t), a^{\nu\dagger}(t')\}\rangle, \\ G^<_{\mu\nu}(t, t') &= i\langle a^{\nu\dagger}(t')a^\mu(t)\rangle, \\ G^>_{\mu\nu}(t, t') &= -i\langle a^\mu(t)a^{\nu\dagger}(t')\rangle. \end{aligned} \qquad (A9)$$

Their equations of motion are given by

$$\begin{aligned} i\left[\boldsymbol{S}\frac{\partial}{\partial t} - \boldsymbol{H}(t)\right]\boldsymbol{G}^{r,a}(t, t') &= \delta(t - t')\boldsymbol{I}, \\ i\left[\boldsymbol{S}\frac{\partial}{\partial t} - \boldsymbol{H}(t)\right]\boldsymbol{G}^{<,>}(t, t') &= \boldsymbol{0}. \end{aligned} \qquad (A10)$$

## APPENDIX B: EFFECT OF TIME-DEPENDENT VOLTAGE

In this section, we consider the effect of adding a time-dependent bias voltage $\Delta_\alpha(t)$ on each lead $\alpha$. The time-dependent Kohn-Sham Hamiltonian is written as

$$h_{ij}(t) = h^0_{ij} + \int dr^3 \delta\upsilon_{KS}(\vec{r}, t)\chi_i^*(\vec{r})\chi_j(\vec{r}), \qquad (B1)$$

where $\boldsymbol{h}^0$ is the equilibrium Kohn-Sham Fock matrix and $\delta\upsilon_{KS}(\vec{r}, t)$ is the induced Kohn-Sham potential caused by the bias voltage. We will assume the followings:

1. The electrodes are non-interacting, thus the exchange-correlation potential is zero inside the leads as well as for lead-device coupling.
2. The screening approximation: $\delta\upsilon_{KS}(\vec{r}, t) = \Delta_\alpha(t)$ for any $\vec{r}$ in the electrodes (thus in both the lead regions and near the lead-device interfaces).

We will show that these two assumptions lead to the homogeneous rigid shift of the surface Green's function and the self-energy. It is noted that assumption (2) is justified by the fact that we always include part of the electrodes in the device region. Now we have $h_{ij}(t) = h^0_{ij} + \Delta_\alpha(t)\int dr^3 \chi_i^*(\vec{r})\chi_j(\vec{r})$ for any $i$ or $j \in \alpha$, leading to

$$\delta\boldsymbol{v}_{KS}(t) = \begin{bmatrix} \boldsymbol{S}_L\Delta_L(t) & \boldsymbol{S}_{LD}\Delta_L(t) & \boldsymbol{0} \\ \boldsymbol{S}_{DL}\Delta_L(t) & \boldsymbol{U}(t) + \delta\boldsymbol{v}_{XC}(t) & \boldsymbol{S}_{DR}\Delta_R(t) \\ \boldsymbol{0} & \boldsymbol{S}_{RD}\Delta_R(t) & \boldsymbol{S}_R\Delta_R(t) \end{bmatrix}, \qquad (B2)$$

where $\boldsymbol{U}(t)$ is evaluated by solving the Poisson equation $\nabla^2 U(\vec{r}, t) = -4\pi\rho(\vec{r}, t)$ and $\delta\boldsymbol{v}_{XC}(t)$ is XC potential for the device region.

With $\boldsymbol{h}_\alpha(t) = \boldsymbol{h}^0_\alpha + \boldsymbol{S}_\alpha\Delta_\alpha(t)$ and $\boldsymbol{h}_{D\alpha}(t) = \boldsymbol{h}^0_{D\alpha} + \boldsymbol{S}_{D\alpha}\Delta_\alpha(t)$, the energy-resolved surface Green's function and self-energy at time $t = t'$ are equal to the equilibrium

ones homogeneously shifted by $\Delta_\alpha(t)$,

$$
g_\alpha^{<,>}(\varepsilon, t, t) = g_\alpha^{<,>}(\varepsilon - \Delta_\alpha(t), 0, 0),
$$
$$
\mathbf{\Sigma}_\alpha^{<,>}(\varepsilon, t, t) = \mathbf{\Sigma}_\alpha^{<,>}(\varepsilon - \Delta_\alpha(t), 0, 0). \tag{B3}
$$

Integrating the equation of motion of $g_\alpha^{<,>}(t, t')$, we have

$$
g_\alpha^{<,>}(t, t') = g_\alpha^{<,>}(t - t') \exp\left[i \int_{t'}^{t} d\tau \, \Delta_\alpha(\tau)\right]. \tag{B4}
$$

Plug it into the expression for self-energy (Eq. (6)), we find

$$
\mathbf{\Sigma}_\alpha^{<,>}(t, t') = \mathbf{\Sigma}_\alpha^{<,>}(t - t') \exp\left[i \int_{t'}^{t} d\tau \, \Delta_\alpha(\tau)\right], \tag{B5}
$$

where $g_\alpha^{<,>}(t - t')$ and $\mathbf{\Sigma}_\alpha^{<,>}(t - t')$ are the ground/equilibrium surface Green's function and self-energy.

## APPENDIX C: EVALUATE $\tilde{S}_D$ AND $\tilde{h}_D$

To propagate the HEOM in non-orthogonal basis, we need to evaluate the "effective" overlap and Fock matrix, $\tilde{S}_D$ and $\tilde{h}_D$, which are related to the original ones, $S_D$ and $h_D$, by

$$
\tilde{S}_D = S_D - \sum_\alpha \mathbf{\Sigma}_\alpha^1,
$$
$$
\tilde{h}_D(t) = h_D(t) + \sum_\alpha \mathbf{\Sigma}_\alpha^0(t), \tag{C1}
$$

where $\mathbf{\Sigma}_\alpha^0(t)$ and $\mathbf{\Sigma}_\alpha^1$ are defined as

$$
\mathbf{\Sigma}_\alpha^0(t) = S_{D\alpha} S_\alpha^{-1} h_\alpha(t) S_\alpha^{-1} S_{\alpha D}
$$
$$
- S_{D\alpha} S_\alpha^{-1} h_{\alpha D}(t) - h_{D\alpha}(t) S_\alpha^{-1} S_{\alpha D},
$$
$$
\mathbf{\Sigma}_\alpha^1 = S_{D\alpha} S_\alpha^{-1} S_{\alpha D}. \tag{C2}
$$

Since we have assumed $h_\alpha(t) = h_\alpha^0 + S_\alpha \Delta_\alpha(t)$ and $h_{D\alpha}(t) = h_{D\alpha}^0 + S_{D\alpha} \Delta_\alpha(t)$ (see Appendix B), $\mathbf{\Sigma}_\alpha^0(t)$ can be written alternatively as

$$
\mathbf{\Sigma}_\alpha^0(t) = \mathbf{\Sigma}_\alpha^0 - \mathbf{\Sigma}_\alpha^1 \Delta_\alpha(t), \tag{C3}
$$

where $\mathbf{\Sigma}_\alpha^0$ is the equilibrium $\mathbf{\Sigma}_\alpha^0(t)$:

$$
\mathbf{\Sigma}_\alpha^0 = S_{D\alpha} S_\alpha^{-1} h_\alpha^0 S_\alpha^{-1} S_{\alpha D}
$$
$$
- S_{D\alpha} S_\alpha^{-1} h_{\alpha D}^0 - h_{D\alpha}^0 S_\alpha^{-1} S_{\alpha D}. \tag{C4}
$$

Therefore, we only need to evaluate beforehand the time-independent quantities $\mathbf{\Sigma}_\alpha^0$ and $\mathbf{\Sigma}_\alpha^1$.

$\mathbf{\Sigma}_\alpha^1 = S_{D\alpha} S_\alpha^{-1} S_{\alpha D}$ can be calculated using standard techniques in evaluating the surface Green's function.[49] Calculation of $\mathbf{\Sigma}_\alpha^0$ is much more difficult since it involves solving the surface block of the semi-infinite dimension matrix equation $S_\alpha X S_\alpha = h_\alpha$. Fortunately, it can be estimated from the real part of self-energy in energy-domain.

By doing a Fourier transform on Eq. (10) with respect to $(t - t') \to E$, we can show that at equilibrium state, $\mathbf{\Sigma}_\alpha^r(E)$ is

given by

$$
\mathbf{\Sigma}_\alpha^r(E) = \mathbf{\Sigma}_\alpha^0 + \mathbf{\Sigma}_\alpha^1 E + \frac{1}{2\pi} \mathcal{P} \int_{-\infty}^{\infty} dE' \frac{\mathbf{\Lambda}_\alpha(E')}{E - E'} - \frac{i}{2} \mathbf{\Lambda}_\alpha(E), \tag{C5}
$$

where $\mathcal{P}$ denotes the Cauchy principal value.

Because $\mathbf{\Lambda}_\alpha(E)$ is non-zero only within a finite range of $E$, $\mathbf{\Sigma}_\alpha^r(E) \to \mathbf{\Sigma}_\alpha^0 + \mathbf{\Sigma}_\alpha^1 E + O(1/E)$ asymptotically as $E \to \pm\infty$. Since we can calculate $\mathbf{\Sigma}_\alpha^r(E)$ explicitly by

$$
\mathbf{\Sigma}_\alpha^r(E) = [E S_{D\alpha} - h_{D\alpha}] g_\alpha^r(E) [E S_{\alpha D} - h_{\alpha D}], \tag{C6}
$$

we can determine $\mathbf{\Sigma}_\alpha^0$, $\mathbf{\Sigma}_\alpha^1$ from the values of $\mathbf{\Sigma}_\alpha^r(E)$ at some very large $E$.

By the way, Eq. (C5) can also be obtained by expanding Eq. (C6) and utilizing the fact that $[(E + i\eta)S_\alpha - h_\alpha] g_\alpha^r(E) = I$, where $\eta \to 0^+$. In this way, Eq. (27) in Sec. II B can also be shown easily,

$$
\tilde{\mathbf{\Sigma}}_\alpha^r(E) = \frac{1}{2\pi} \mathcal{P} \int_{-\infty}^{\infty} dE' \frac{\mathbf{\Lambda}_\alpha(E')}{E - E'} - \frac{i}{2} \mathbf{\Lambda}_\alpha(E)
$$
$$
= \tilde{h}_{D\alpha} g_\alpha^r(E) \tilde{h}_{\alpha D}. \tag{C7}
$$

## APPENDIX D: INITIAL VALUES FOR HEOM

Proper initial values for RSDM, 1st and 2nd tier ARSDM are essential for the propagation of HEOM to produce physically correct results. Here, the system is assumed to be initially in the equilibrium state. In this case, the RSDM, 1st and 2nd tier ARSDM keep unchanged as long as no bias voltage is applied (i.e., $\dot{\sigma}_D = \dot{\varphi}_{\alpha,k} = \dot{\varphi}_{\alpha,k,\alpha',k'} = 0$). And the electrons occupy the single-particle states according to the Fermi-Dirac distribution so that

$$
G_D^<(E) = -2i f(E - \mu) \text{Im} G_D^r(E),
$$
$$
G_D^>(E) = 2i \left[1 - f(E - \mu)\right] \text{Im} G_D^r(E), \tag{D1}
$$

where $\mu$ is the chemical potential at equilibrium. The equilibrium RSDM can be calculated by a semi-circular contour integral of $G_D^r(E)$ on the upper complex plane,

$$
\sigma_D = -\frac{1}{\pi} \text{Im} \left[\int_{-\infty}^{\infty} dE f(E - \mu) G_D^r(E)\right]
$$
$$
= -\frac{1}{\pi} \text{Im} \left[\int_C dE f(E - \mu) G_D^r(E) + \sum_p R_p G_D^r(\zeta_p)\right], \tag{D2}
$$

where $C$ is a semi-circular contour on the upper complex plane and $\zeta_p = \mu + iz_p$ and $-R_p$ are the $p^{\text{th}}$ Padè pole and residue of the Fermi function, respectively. The summation runs through all singularities lying between the semi-circle and real axis.

The equilibrium 1st tier ARSDM can be evaluated by residue theorem since the semi-circle contour integral trends

to zero when its radius trends to infinity,

$$
\begin{aligned}
\boldsymbol{\varphi}_{\alpha,k} &= \frac{1}{2\pi} \int_{-\infty}^{\infty} dE \Bigg[ \frac{1}{E - \varepsilon_{\alpha,k}} \boldsymbol{G}_D^<(E) \boldsymbol{A}_{\alpha,k}^{>+} \\
&\quad - \frac{1}{E - \varepsilon_{\alpha,k}} \boldsymbol{G}_D^>(E) \boldsymbol{A}_{\alpha,k}^{<+} \Bigg] \\
&= \frac{i}{2\pi} \int_{-\infty}^{\infty} dE \Bigg[ \frac{i \left[ \boldsymbol{G}_D^r(E) - \boldsymbol{G}_D^a(E) \right] \boldsymbol{A}_{\alpha,k}^{<+}}{E - \varepsilon_{\alpha,k}} \\
&\quad + \frac{f(E - \mu) \left[ \boldsymbol{G}_D^r(E) - \boldsymbol{G}_D^a(E) \right] \boldsymbol{\Lambda}_{\alpha,k}}{E - \varepsilon_{\alpha,k}} \Bigg] \\
&= - \boldsymbol{G}_D^r(\varepsilon_{\alpha,k}) \left[ i \boldsymbol{A}_{\alpha,k}^{<+} + f(\varepsilon_{\alpha,k} - \mu) \boldsymbol{\Lambda}_{\alpha,k} \right] \\
&\quad - 2 \sum_{p=1}^{N_p} \left[ \varepsilon_{\alpha,k}^* \mathrm{Re}(\boldsymbol{\Xi}_{\alpha,k,p}) - \mathrm{Re}\left( \zeta_p \boldsymbol{\Xi}_{\alpha,k,p} \right) \right] \boldsymbol{\Lambda}_{\alpha,k}.
\end{aligned}
$$

(D3)

In the last equality, the first term corresponds to the residue at $E = \varepsilon_{\alpha,k}$ while the second term corresponds to the residues of Fermi function. $\varepsilon_{\alpha,k}^*$ is the complex conjugate of $\epsilon_{\alpha,k}$ and $\Xi_{\alpha,k,p}$ is the short-hand notation for

$$
\boldsymbol{\Xi}_{\alpha,k,p} = \frac{R_p}{\left( \zeta_p - \varepsilon_{\alpha,k} \right) \left( \zeta_p - \varepsilon_{\alpha,k}^* \right)} \boldsymbol{G}_D^r(\zeta_p).
$$

(D4)

Once the 1st tier ARSDM are known, initial values for 2nd tier ARSDM $\boldsymbol{\varphi}_{\alpha,k,\alpha',k'}$ can be evaluated directly by requiring them to satisfy $\frac{d}{dt} \boldsymbol{\varphi}_{\alpha,k,\alpha',k'}(t) = 0$. This gives

$$
\boldsymbol{\varphi}_{\alpha,k,\alpha',k'} = \frac{\boldsymbol{\Lambda}_{\alpha',k'} \boldsymbol{\varphi}_{\alpha,k} - \boldsymbol{\varphi}_{\alpha',k'}^\dagger \boldsymbol{\Lambda}_{\alpha,k}}{\varepsilon_{\alpha,k} - \varepsilon_{\alpha',k'}^*}.
$$

(D5)

It is noted that the denominator is always non-zero since $\mathrm{Im}\left[ \varepsilon_{\alpha,k} \right] > 0$ for any $\alpha$ and $k$, which can be seen from Eqs. (40) and (41).

With the proper initial values for $\boldsymbol{\sigma}_D$, $\boldsymbol{\varphi}_{\alpha,k}$, $\boldsymbol{\varphi}_{\alpha,k,\alpha',k'}$, we can then propagate the HEOM to obtain the time-dependent $\boldsymbol{\sigma}_D(t)$, $\boldsymbol{\varphi}_{\alpha,k}(t)$, $\boldsymbol{\varphi}_{\alpha,k,\alpha',k'}(t)$.

[1]M. Auf der Maur, M. Povolotskyi, F. Sacconi, A. Pecchia, G. Romano, G. Penazzi, and A. Di Carlo, Opt. Quantum Electron. **40**, 1077 (2008).
[2]M. A. Reed, C. Zhou, C. J. Muller, T. P. Burgin, and J. M. Tour, Science **278**, 252 (1997).
[3]H. Song, Y. Kim, Y. H. Jang, H. Jeong, M. A. Reed, and T. Lee, Nature (London) **462**, 1039 (2009).
[4]H. Song, M. A. Reed, and T. Lee, Adv. Mater. **23**, 1583 (2011).
[5]S. W. Wu, N. Ogawa, and W. Ho, Science **312**, 1362 (2006).
[6]M. Galperin and A. Nitzan, Phys. Chem. Chem. Phys. **14**, 9421 (2012).
[7]A. Nitzan and M. A. Ratner, Science **300**, 1384 (2003).
[8]T. Fujisawa, D. G. Austing, Y. Tokura, Y. Hirayama, and S. Tarucha, J. Phys.: Condens. Matter **15**, R1395 (2003).
[9]X. Zheng, F. Wang, C. Y. Yam, Y. Mo, and G. H. Chen, Phys. Rev. B **75**, 195127 (2007).
[10]X. Zheng, G. H. Chen, Y. Mo, S. K. Koo, H. Tian, C. Y. Yam, and Y. J. Yan, J. Chem. Phys. **133**, 114101 (2010).
[11]G. Stefanucci and C. O. Almbladh, Europhys. Lett. **67**, 14 (2004).
[12]G. Stefanucci and C. O. Almbladh, Phys. Rev. B **69**, 195318 (2004).
[13]S. Kurth, G. Stefanucci, C.-O. Almbladh, A. Rubio, and E. K. U. Gross, Phys. Rev. B **72**, 035308 (2005).
[14]M. Koentopp, C. Chang, K. Burke, and R. Car, J. Phys.: Condens. Matter **20**, 083203 (2008).
[15]M. Galperin and S. Tretiak, J. Chem. Phys. **128**, 124705 (2008).
[16]S.-H. Ke, R. Liu, W. Yang, and H. U. Baranger, J. Chem. Phys. **132**, 234105 (2010).
[17]J. Maciejko, J. Wang, and H. Guo, Phys. Rev. B **74**, 085324 (2006).
[18]Y. Xing, B. Wang, and J. Wang, Phys. Rev. B **82**, 205112 (2010).
[19]K. Burke, R. Car, and R. Gebauer, Phys. Rev. Lett. **94**, 146803 (2005).
[20]E. J. McEniry, D. R. Bowler, D. Dundas, A. P. Horsfield, C. G. Sánchez, and T. N. Todorov, J. Phys.: Condens. Matter **19**, 196201 (2007).
[21]J. Jin, X. Zheng, and Y. Yan, J. Chem. Phys. **128**, 234703 (2008).
[22]Y. Zhang, S. G. Chen, and G. H. Chen, Phys. Rev. B **87**, 085110 (2013).
[23]H. Xie, F. Jiang, H. Tian, X. Zheng, Y. H. Kwok, S. G. Chen, C. Y. Yam, Y. Yan, and G. H. Chen, J. Chem. Phys. **137**, 044113 (2012).
[24]H. Tian and G. H. Chen, J. Chem. Phys. **137**, 204114 (2012).
[25]K. Cho, T. A. Arias, J. D. Joannopoulos, and P. K. Lam, Phys. Rev. Lett. **71**, 1808 (1993).
[26]R. A. Lippert, T. Arias, and A. Edelman, J. Comput. Phys. **140**, 278 (1998).
[27]L. Genovese, A. Neelov, S. Goedecker, T. Deutsch, S. A. Ghasemi, A. Willand, D. Caliste, O. Zilberberg, M. Rayson, A. Bergman, and R. Schneider, J. Chem. Phys. **129**, 014109 (2008).
[28]J. M. Soler, E. Artacho, J. D. Gale, A. García, J. Junquera, P. Ordejón, and D. Sánchez-Portal, J. Phys.: Condens. Matter **14**, 2745 (2002).
[29]D. R. Bowler and T. Miyazaki, Rep. Prog. Phys. **75**, 036503 (2012).
[30]S. Kim and N. Marzari, Phys. Rev. B **87**, 245407 (2013).
[31]N. Marzari, A. A. Mostofi, J. R. Yates, I. Souza, and D. Vanderbilt, Rev. Mod. Phys. **84**, 1419 (2012).
[32]J. Taylor, H. Guo, and J. Wang, Phys. Rev. B **63**, 245407 (2001).
[33]Y. Xue, S. Datta, and M. A. Ratner, Chem. Phys. **281**, 151 (2002).
[34]G. Autès, C. Barreteau, D. Spanjaard, and M.-C. Desjonquères, Phys. Rev. B **77**, 155437 (2008).
[35]I. Rungger and S. Sanvito, Phys. Rev. B **78**, 035407 (2008).
[36]A. R. Rocha, V. M. García-Suárez, S. Bailey, C. Lambert, J. Ferrer, and S. Sanvito, Phys. Rev. B **73**, 085414 (2006).
[37]J. K. Viljas, J. C. Cuevas, F. Pauly, and M. Häfner, Phys. Rev. B **72**, 245415 (2005).
[38]J. Fransson, O. Eriksson, and I. Sandalov, Phys. Rev. B **66**, 195319 (2002).
[39]K. S. Thygesen, Phys. Rev. B **73**, 035309 (2006).
[40]E. Runge and E. K. U. Gross, Phys. Rev. Lett. **52**, 997 (1984).
[41]J. Hu, R.-X. Xu, and Y. J. Yan, J. Chem. Phys. **133**, 101106 (2010).
[42]M. Elstner, D. Porezag, G. Jungnickel, J. Elsner, M. Haugk, T. Frauenheim, S. Suhai, and G. Seifert, Phys. Rev. B **58**, 7260 (1998).
[43]Y. Wang, C. Y. Yam, T. Frauenheim, G. H. Chen, and T. A. Niehaus, Chem. Phys. **391**, 69 (2011).
[44]W. Kohn and L. J. Sham, Phys. Rev. **140**, A1133 (1965).
[45]A.-P. Jauho, N. S. Wingreen, and Y. Meir, Phys. Rev. B **50**, 5528 (1994).
[46]E. Khosravi, A.-M. Uimonen, A. Stan, G. Stefanucci, S. Kurth, R. van Leeuwen, and E. K. U. Gross, Phys. Rev. B **85**, 075103 (2012).
[47]C. G. Sánchez, M. Stamenova, S. Sanvito, D. R. Bowler, A. P. Horsfield, and T. N. Todorov, J. Chem. Phys. **124**, 214708 (2006).
[48]E. Khosravi, G. Stefanucci, S. Kurth, and E. Gross, Phys. Chem. Chem. Phys. **11**, 4535 (2009).
[49]M. P. L. Sancho, J. M. L. Sancho, J. M. L. Sancho, and J. Rubio, J. Phys. F **15**, 851 (1985).